Coastal Dynamics 2017
Paper No. 060

A NUMERICAL STUDY OF EXTREME WAVE RUNUP BEHAVIOR: SPECTRAL AND STATISTICAL ANALYSIS

Alexandre Nicolae Lerma[1], Thomas Bulteau[2]

Abstract

A numerical study using SWASH model is realized on a multi-barred beach in order to explore spectral and statistical behavior of wave runup caused by moderate to extreme offshore wave conditions. Numerical experiments based on bathymetric characteristics, wave climate and tidal level of the Aquitanian coast, are compared to collected field data from the bibliography and derivate parametric models. Correlations between runup and several environmental parameters are estimated and discussed and a hybrid model (based on observations and simulated results) is proposed. We analyse the longshore spatial variability of incident and infragravity swash heights and $R_{2\%}$, in order to identify hot spot of runup related to the near shore morphology. Depending on wave conditions and tidal level, local positive anomaly of $R_{2\%}$ varies between 10 to 36 % and are in average 22% higher than longshore mean values at high tide.

Key words: hot spot of runup, swash energy spectra, extreme wave conditions, multi-barred beach, longshore variability, SWASH model

1. Introduction

The runup, defined as the maximum shoreline vertical elevation, is a dynamic process representing the edge of the sea and land interface on the beach. Estimating runup value is fundamental for coastal risks studies as well as for engineering studies or structure resistance and design. It is therefore a major issue in coastal studies as evidenced by the considerable bibliography on this topic and the multiple approaches used to estimate runup. Nevertheless, runup observations on open beaches during storms are scarce, mainly due to the difficulties to maintain hydrodynamic measuring devices in the swash zone because of wave energy and strong currents. Video observations from the beach or the dune frequently suffer extremes atmospheric conditions, wind and rain can prevent acquisitions or alter the quality of measurements. As a result, the most frequently used parametric estimations for runup are derived from observed runup data set for offshore wave conditions inferior to Hs = 4 m and Tp = 15 s (Holman, 1986; Stockdon et al., 2006). To the authors' knowledge, runup observations obtained under the most energetic conditions (Hs = 6.4 m and Tp = 16.4 s) were analyzed in Senechal et al. (2011). For moderate wave conditions, runup was reported to be dependent on offshore wave conditions and foreshore beach slope. It is generally related to the Irribaren number (Miche, 1959; Battjes, 1974) or a non-dimensional equivalent form (Sallenger and Holman, 1985; Stockdon et al., 2006). In contrast, the observation in highly dissipative conditions presents better correlations when the runup is scaled by the significant wave height (Hs) or $(HoLo)^{1/2}$, considering $Hs \approx Ho$ and Lo the wave length in deep water (Ruessink et al., 1998; Ruggiero et al., 2004; Stockdon et al., 2006; Senechal et al., 2011).

The shoreline motion on the beach also is commonly studied in terms of spectra frequencies spectrum. Conventional delimitation used for convenience to delimit short wave from local wind and swell and infragravity waves including standing and edges wave is 0.05Hz (e.g. Guza and Thornton, 1982). On reflective and intermediate beach state, swash energy is supposed to be more concentrated in short wave than long wave frequencies, whereas on dissipative beach there are more energy in the long wave band (Hughes et al., 2014). Generally, the energy contained in the wave energy spectra increases with stronger deep water wave conditions. Nevertheless, depending on beach characteristics like beach slope, near shore bar morphology water level, the structure of the spectra in short wave bands and infragravity bands can be highly variable. Many studies showed that short wave swash energy remains roughly constant due to saturation caused by wave breaking (e.g. Guza and Thornton, 1982; Aagaard, 1990). These studies reported that swash spectra display an f^{-3} or f^{-4} dependence at wind wave frequencies and energy density in the roll

[1]BRGM (French Geological Survey), Risks and Prevention Division - Coastal Risks and Climate Change Unit, Orléans, France
[2]BRGM (French Geological Survey), Regional Direction Nouvelle-Aquitaine - Pessac, France,

off band is related to beach gradient alone (Guza and Thornton, 1982; Ruessink et al., 1998; Ruggiero et al., 2004, Hughes et al., 2014). In opposition, the infragravity swash was observed to be highly variable in form, across all beach-states and presents no significant relation to beach slope (Ruessink et al., 1998; Stockdon et al., 2006; Senechal et al., 2011). Many different behaviors were observed like predominant white spectra (Ruessink et al., 1998), significant peaks related to leaky mode standing waves or edge waves (Aagaard, 1990) or under highly energetic conditions, extension off the spectral energy roll off into the long wave bands (Ruessink et al., 1998; Ruggiero et al., 2004; Senechal et al., 2011). The signatures of standing waves or edge waves in the infragravity spectra were attributed to selective amplification of particular frequencies probably due to resonant interaction with near shore morphology (e.g. Kirby et al., 1981; Wright, 1982; Hughes et al., 2014). Depending on the beach state, peaks frequencies are supposed to manifest on reflective beach at the first sub-harmonic, related to sub-harmonic standing edge waves (Wright, 1982). On intermediate beach the infragravity swash band is expected to be peaky structured due to amplification of edges waves and shore normal surf beat, (Wright, 1982; Hughes et al., 2014). With increasing wave conditions the infragravity swash spectra become featureless. This absence of peak is supposed to be due to generally less marked morphology on dissipative beach preventing preferential amplification and resonance (Hughes et al., 2014).
In this study we analyze the runup behavior under increasing wave conditions from moderate to extreme using the numerical model SWASH (Zijlema et al., 2011). Parametric runup, swash energy spectra and alongshore spatial variability are analyze in relation with complex near-shore bathymetric morphology.

2. Site and methods

2.1. *Bathymetry*

The Truc Vert beach is a high-energy open beach on the south-western French Atlantic coast, mainly north to south oriented. The Truc Vert beach morphology often involves two distinct sandbar systems. The inner bar can appear in all states of the intermediate beach classification (see Wright and Short, 1984; Masselink and Short, 1993) and usually exhibits a Transverse Bar and Rip morphology (Senechal et al., 2011). The outer bar system exhibits persistent long-term crescent-shaped patterns that vary from symmetrical to asymmetrical (Castelle et al., 2007).

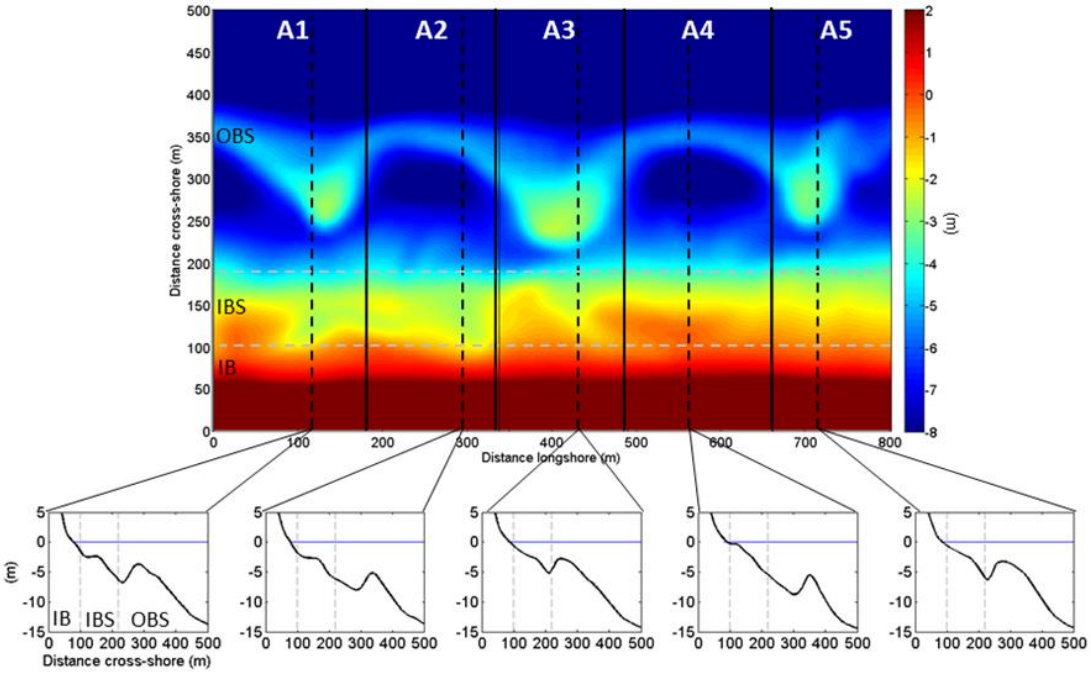

Figure 1 : Bathymetry used for simulation and analysis (data collected during the ECORS-Truc Vert'08 beach experiment from a complete topo-bathymetric survey (Sénéchal et al., 2011). Spatial resolution of the topo bathymetric model is 2 m. The domain is divided in 5 sub domains (A1 to A5) presenting variable combination of Outer Bar System (OBS), Inner Bar System (IBS) and Intertidal Beach (IB) morphological characteristics. Morphological configurations are detailed in the text. Dashed lines locate a representative cross-shore profile of the main

characteristics of each sub-domain.

This complex, three-dimensional morphology is here divided for analysis in 5 sub-domains (A1 to A5, cf. figure 1), presenting variable combination of Outer Bar System (OBS), Inner Bar System (IBS) and Intertidal Beach (IB) morphological and beach slope characteristics (Intertidal Beach slope noted β_{IB} is calculated between mean sea level 0.36 m/NGF (French topographic reference) and high spring tide level 2.23m/NGF).

- A1 exhibits a horn of the OBS, a north-south oriented deep rip channel in the IBS and a IB mean beach slope $\overline{\beta}_{IB} = 0.094$ and $\beta_{IB,\,max} = 0.11$
- A2 is characterized by deep trough in the OBS, a south-north oriented deep rip channel in the IBS and $\overline{\beta}_{IB} = 0.086$ and $\beta_{IB,\,max} = 0.098$
- A3 exhibits a massive horn in the OBS, a south-north oriented shallow rip channel, $\overline{\beta}_{IB}=0.08$ and $\beta_{IB,\,max}=0.085$
- A4 is characterized by deep trough in the OBS, and a sand bar at the IBS, $\overline{\beta}_{IB} = 0.078$ and $\beta_{IB,\,max} = 0.085$
- A5 exhibits a horn at the OBS, a nearly uniform slope at the IBS around 0.04 and, $\overline{\beta}_{IB} = 0.09$ and $\beta_{IB,\,max} = 0.098$.

This classification based on qualitative and quantitative morphological criteria (beach slope) was used in order to further analyze longshore runup variability.

2.2. *Model settings*

Simulations are performed with the SWASH model, (Zijlema et al., 2011) in a multilayered (2 vertical layers) 2D mode on a 2.2x2.2 km² domain (2 m spatial resolution). The simulation time for each case is set to 22 min, with a 7 minutes spin-up, and outputs are stored every second. As recalled in introduction, field runup observation data are scarce and so model performance validation in case of realistic field conditions are only partial. Nevertheless, in the case of Truc Vert site, Nicolae Lerma et al., 2017, show good performance of SWASH model in 2D configuration simulating wave setup and runup during the storm Johanna. Model performance was validated comparing simulations with observations of wave setup for the following conditions: *Hs* = 8.2 m and *Tp* = 18.3 s and wave runup for the following conditions: *Hs* = 6.4 m and Tp = 16.4 s. With identical model setting to the one of the present study, the significant swash height (*S*) was fairly well reproduced with a coefficient of determination ρ^2 =0.71, RMSE=0.43 m and $R_{2\%}$ was even better reproduced with ρ^2 = 0.78, RMSE = 0.34 m and a Mean Absolute Percentage Error, MAPE=13.2%. For further details see, Nicolae Lerma et al., 2017.

2.3. *Forcing*

The wave climate on the Aquitanian coast is energetic, characterized by a mean annual significant wave height of 1.7 m, a mean annual peak period of 10.3 s and severe North Atlantic storms that episodically cause Hs to exceed 8 m (from observations at the Cap Ferret Buoy, in Castelle et al., 2015). Simulations performed in order to cover moderate to extreme wave conditions. To proceed, we simulate 4 cases representing progressive increasing wave conditions from *Hs*=2 m to 8 m and *Tp*=8 s to 20 s. These conditions are considered respectively as moderately energetic being near to annual mean conditions (*Hs*=2 m and *Tp*=8 s), highly energetic near to the threshold defining the beginning of a storm event at cap Ferret buoy in Castelle et al., 2015 (i.e. *Hs*=4 m and *Tp*=12 s), storm regime corresponding to a classical storm conditions (annual return period, *Hs*=6m and *Tp*=16 s) and extremely energetic near to a Hs 10-year return period event for this part of the Aquitanian coast in Nicolae Lerma et al., 2015 (i.e. *Hs* = 8 m and *Tp* = 20 s). The Aquitanian coast is a meso-macrotidal coast, the tide is semidiurnal with an annual mean spring tide range of 3.7 m around Truc Vert site. In order to analyse the influence of water level on runup behavior, water levels were set at 0m/NGF (mid tide), 1m/NGF and 2 m/NGF (high tide).

Table 1. Forcing conditions.

Event	Case	Wlev	Hs	Tp
Moderate	1;5;9	0;1;2	2	8
High	2;6;10	0;1;2	4	12

Stormy	3;7;11	0;1;2	6	16
Extreme	4;8;12	0;1;2	8	20

2.4. *Post-treatment*

For each case, results are post-processed along 800 cross-shore transects at the center of the domain. The shoreline vertical elevation values η are extracted every second, tracking the water line as the last wet cell where current values are null. Wave setup is calculated as the time-averaged water-level elevation at the shoreline during 15 min and is noted hereinafter $\langle\eta\rangle$. The value of η exceeded 2% of the time (denoted $R_{2\%}$), can be calculated using several methods (Holman, 1986). Here the $R_{2\%}$ exceedance was derived considering the cumulative distribution function of the entire water-level time series during 15 min. The significant swash height (S) is calculated for all cross-shore profiles, computing the power spectra density, PSD (f), from detrended, tapered shoreline vertical elevation time series as:

$$\mathbf{S = 4 * \sqrt{\sum PSD(f)df}} \quad (1)$$

Swash heights in the incident band component (0.05 Hz < f < 0.24 Hz) and in the infragravity band component (0.004 Hz < f < 0.05 Hz) are calculated by summing only frequencies within the specified limits, and are noted S_{inc} and S_{ig} respectively.

3. Results

3.1. *Incident, infragravity swash and Runup 2% exceedance*

Usually the beach state is defined by the Iribarren number (Battjes, 1974) noted:

$$\xi = \frac{\beta}{(Ho/Lo)0.5} \quad (3)$$

relating off-shore wave characteristics with the local foreshore slope. Beach slope β is here calculated as the average slope over a region within $\langle\eta\rangle \pm 2$ standard deviation of the continuous water level motion. The traditional beach classification indicates dissipative conditions for ξ <0.3, intermediate for 0.3< ξ <1.25 and reflective if ξ >1.25 (Wright and Short, 1984). In addition, the ratio S_{inc}/S_{ig} indicates the predominant conditions contributing to runup (see fig. 2). If S_{inc}/S_{ig} < 1, runup is dominated by the infragravity frequencies band, if S_{inc}/S_{ig} >1 runup is dominated by the incident frequencies band.

Infragravity dominated runup motion is mostly observed on dissipative beaches (Ruessink et al., 1998; Ruggiero et al., 2004; Stockdon et al., 2006). Under energetic conditions for an equivalent beach slope, conditions are supposed to tend to be dissipative. Nevertheless due to general steep slope in the Truc Vert beach $\overline{\beta}_{IB}$=0.086, conditions are generally intermediate and tend to be reflective at high tide (slope in the upper beach being almost steeper). On the one hand, results in figure 2 suggest that shoreline motions can be dominated by the infragravity frequencies band even if the Iribarren number indicates intermediate or reflective conditions. This is mostly the case under storm condition at high tide when wave interact with the upper beach (case 10, 11 12, cf. table 1). On the other hand, as suggested by Ruessink et al., 1998 and Senechal et al., 2011, the use of the Iribarren number related to the local foreshore slope may not be relevant to characterize storm regime where beach profiles are complex.

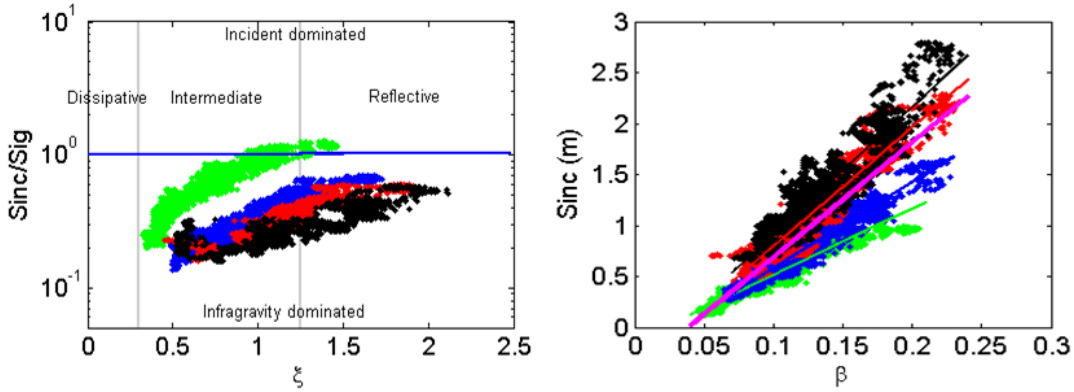

Figure 2 : Left panel, ratio of incident to infragravity swash plotted against the Iribarren number noted ξ. Results for mid tide, mid-tide + 1m and high tide are plotted together, green for moderate conditions, blue for high conditions, red for storm conditions and black for extreme conditions. The vertical dashed lines mark the cutoff values between dissipative conditions ξ<0.3, intermediate 0.3< ξ<1.25, reflective ξ>1.25. Values above the horizontal line at $S_{inc}/S_{ig}=1$ are incident dominated while those below the line are infragravity dominated. On the right panel, local beach slope β is plotted against the incident swash (S_{inc}) for all cases. Lines represent the best linear regression for each forcing conditions event, with the magenta line for all data considered together. Details on linear regressions are presented in table 2.

Incident swash has been reported in many studies to be related to local beach slope (see Hugues et al 2014 for a review), even in dissipative conditions (e.g. Ruggiero et al 2004, Senechal et al., 2011). Our results concur with these finding presenting a very strong linear relation between S_{inc} and β for all wave conditions (figure 2). We note that with increasing offshore wave conditions, the slope of the linear regression increases as the value of the intercept (see table 2)

Table 2. Relation between S_{inc} and local beach slope.

Event	Dependent variable	Explicative variable	Slope	Intercept	ρ^2	RMSE(cm)
Moderate	S_{inc}	β	6.5(±0.04)	-0.13	0.920	0.069
High	S_{inc}	β	8.4(±0.04)	-0.26	0.935	0.084
Stormy	S_{inc}	β	11.7(±0.08)	-0.37	0.893	0.144
Extreme	S_{inc}	β	12.6(±0.11)	-0.34	0.853	0.177
All	S_{inc}	β	11.3(±0.07)	-0.44	0.745	0.252

Infragravity swash is better scaled by *Hs* or $(HoLo)^{1/2}$. Figure 3 illustrates S_{ig} and $R_{2\%}$ related to *Hs* and $(HoLo)^{1/2}$ for increasing wave energy conditions. The results from simulation (longshore mean value and longshore variability) are compared with data collected during several experiments on barred open beaches mostly during energetic conditions, Duck82, Delilah, Duck94, Sandy Duck, Agate beach, Glenden. For all details about these data sets, see Stockdon et al., 2006. Observed runup from ECORS - Truc Vert experiment are also included for comparison. Wave conditions related to runup observations are reverse shoaled. Comparison is also made with several parametric models from the bibliography based on observations or numerical simulations.
First we observe that for moderate and for highly energetic wave conditions, simulated results are of the same order of magnitude than observations. Scaling by $(HoLo)^{1/2}$ appears to reduce dispersion of the distribution of observations in comparison with Hs. Models from the bibliography generally underestimate simulated values from storm and extreme conditions. Surprisingly the model proposed by Guza and Thornton, 1982 estimates relatively well mean longshore $R_{2\%}$ (Figure 3, (5)).

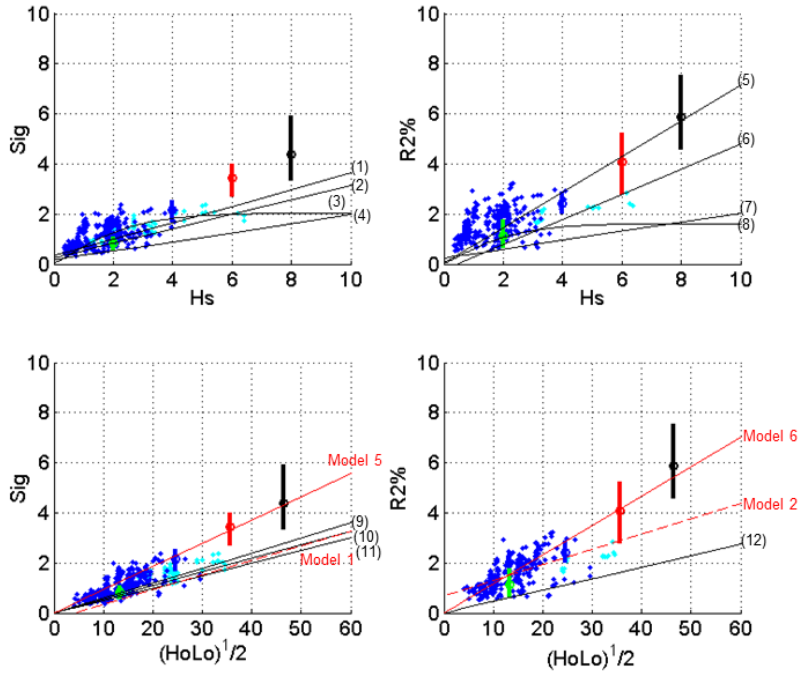

Figure 3 : Simulation results for 12 cases from moderate to extreme offshore wave conditions and comparison with parametric models from the bibliography. Full circles represent longshore mean for the three water level and vertical bar the longshore varibility for moderate conditions (green), for high conditions (blue), for storm conditions (red) and for extreme conditions (black). Blue point represents runup observations from several open barred beach dataset (see text for details), cyan points are observations from Truc Vert campaign. Plotted model form the bibliography for S_{ig} vs Hs: (1) Ruggiero et al., 2001, (2) Birkkemper et al., 2013; (3) Sénéchal et al., 2011, (4) Ruessink et al., 1998; $R_{2\%}$ vs Hs : (5) Guza and Thornton, (6) Ruggiero et al., 2001; (7) Ruessink et al., 1998; (8) Brikkemper et al., 2013., for Sig vs (HoLo)½ : (9) Stockdon et al., 2006; (10) Cox et al., 2013; (11) Sénéchal et al., 2011; for $R_{2\%}$ vs (HoLo)½ : (12) Stockdon et al., 2006. References of models 1,2 5 and 6 are presented in table 3.

Using linear models based on the relation between $(HoLo)^{1/2}$ and observations only (Model1 for S_{ig} and Model2 for $R_{2\%}$, produce a reasonable estimation of $\overline{S}_{ig}$ and $\overline{R}_{2\%}$ for moderate and high conditions. For example $\overline{R}_{2\%}$ is underestimated by 0.22 m for high conditions. However, for storm and extreme conditions, $\overline{R}_{2\%}$ is considerably underestimated by 1.19 m and 2.33 m respectively. Model3 and Model4 are linear models only based on simulations results. In order to evaluate the model performance relations were established only for $(HoLo)^{1/2} > 10$ m² to prevent unrealistic estimation (negative estimation). They present a weak capacity to explain observed data on open barred beach particularly for $\overline{R}_{2\%}$ estimation (cf. table 3). Models based on simulations results and forced by the origin in order to avoid nonphysical intercept (Model 5 and Model 6) improves significantly the correlation between the prediction and the joint distribution of observations and simulations. Errors appear to be reasonable relative to energy conditions and potential spatial variability with RMSE = 0.5 m for $\overline{R}_{2\%}$ (see section 3.2). Considering our results, it is clear that $\overline{S}_{ig}$ and $\overline{R}_{2\%}$ under storm and extreme conditions are not fully following the same tendency than observations on several barred beach, including observation at Truc Vert beach. Although being specifically elaborated to estimate $\overline{S}_{ig}$ and $\overline{R}_{2\%}$ under storm conditions, the models Model5 and Model6 perform quite well to reproduce observed runup under moderate and highly energetic conditions. They are valuable for shore normal incident wave and can be useful as first approximation to estimate mean longshore S_{ig} and $R_{2\%}$ under highly energetic to extreme conditions for Hs>4m and Tp>12s (or $(HoLo)^{1/2}$ > 25m) :

$$S_{ig} = 0.093\sqrt{\mathrm{HoLo}} \tag{3}$$

$$R_{2\%} = 0.117\sqrt{\mathrm{HoLo}} \tag{4}$$

Table 3. Relation between S_{ig}, $R_{2\%}$ and $(HoLo)^{1/2}$

Parametric model	Dependent variable	Explicative variable	Data	Slope	Intercept	ρ^2	RMSE(cm)
Model1	S_{ig}	$(HoLo)^{1/2}$	observations	0.059(±0.003)	0.25	0.57	0.31
Model2	$R_{2\%}$	$(HoLo)^{1/2}$	observations	0.062(±0.005)	0.68	0.37	0.48
Model3	S_{ig}	$(HoLo)^{1/2}$	Simulation	0.107(±0.005)	-0.53	0.99	0.11
Model4	$R_{2\%}$	$(HoLo)^{1/2}$	Simulation	0.144(±0.008)	-0.96	0.99	0.21
Model5	S_{ig}	$(HoLo)^{1/2}$	Simulation	0.093(±0.004)	0	0.99	0.25
Model6	$R_{2\%}$	$(HoLo)^{1/2}$	Simulation	0.117(±0.007)	0	0.99	0.45

3.2. *Longshore variability*

The longshore variability of S_{inc}, S_{ig}, $R_{2\%}$ is illustrated in figure 4 in order to comment the relation between topo-bathymetric morphology (delimited by 5 sub domains A1 to A5) and evaluate potential hot spot of runup (defined as significantly higher local value of runup relative to mean longshore value). The figure represents the difference between the local values of S_{inc}, S_{ig}, $R_{2\%}$ and the respective longshore mean values.

Considering the swash heights in the incident and the infragravity frequencies bands, we observe that the increase in water level is responsible for an accentuated longshore variability (difference between longshore min and max anomaly, see fig 4). More particularly for $S_{inc,}$ we observe a positive anomaly in the rip channel in A1 and A2. This local increase is mostly related to the local beach slope (e.g. at mid-tide, steeper at the beginning of rip channels, 13 %, lower in the area A4 around 6 % and around 9 % in A5). The maximum difference is observed for extreme wave conditions in A1 at high tide were $S_{inc,max}$ is 1m higher than longshore mean values $\overline{S}_{inc}$ and more than 1.5 m higher than S_{inc} in A4 and A5.

For S_{ig} the spatial variability appears to be partly related to the bar and trough configuration of the outer bar system. According to (Guedes et al 2012), the presence of complex sandbar morphology is responsible for non-uniform alongshore breaking wave pattern and so energy dissipation along the surf zone is highly variable due to offshore bar morphology. Whatever the water level, the A2 area, morphologically characterized by a deep trough, presents a clear positive anomaly reaching more than 1m for offshore extreme wave conditions. On the opposite, the A3 area presents systematically the lower values (around -0.5 m). In A1, A4 and A5 the relation with the characteristics of the OBS is less clear. Surprisingly a notable peak appears in A5 for storm and extreme conditions at mid tide and mid tide level + 1m. These higher values are possibly caused by a resonant standing waves favored by an important reflection due to the almost uniform steep slope in the IBS and the IB and a horn in the OBS.

Simulations show that, for equivalent offshore wave conditions $\overline{S}$ increases with the water level. For moderate wave conditions $\overline{S}$ increases about 54 % and S_{max} about 44% between mid and high tide (Table 4). For extreme wave conditions $\overline{S}$ increases by 33 % and S_{max} by 25 %. Due to the non-linearity of the interaction between wave and morphology, the increase for high and storm conditions are important but notably lower respectively 17 % and 19 % for $\overline{S}$ and 16 % and 12 % for S_{max}. These results are consistent with findings of Senechal et al. (2014) on the Truc vert beach. They find for low to moderate wave conditions a reduction of S by 30 % due to sandbar-induced wave breaking at low tide.

The maximum positive anomaly also called hot spot of runup remains almost constant between 10 and 20% of $\overline{S}$. For extreme wave conditions the difference between $\overline{S}$ and S_{max} is around 20 % and remains stable from mid tide to high tide.

Table 4. Mean and longshore max values of S_{inc}, S_{ig}, $R_{2\%}$

Tide	Off shore wave energy	$\overline{R}_{2\%}$ (m)	$R_{2\%,\,max}$ (m)	$\overline{S}$ (m)	S_{max} (m)	$\overline{S}_{ig}$ (m)	$S_{ig,\,max}$ (m)	$\overline{S}_{inc}$ (m)	$S_{inc,\,max}$ (m)	$\overline{S}_{ig}/\overline{S}_{inc}$ (%)	$\Delta(\overline{S}_{ig}/\overline{S}_{inc})$ (%)
Mid tide	moderate	0.90	1.20	0.85	1.07	0.79	0.96	0.26	0.42	0.93	0.11
	high	2.30	2.60	2.20	2.57	2.14	2.52	0.42	0.61	0.98	0.04
	storm	3.38	3.76	3.46	4.09	3.31	3.94	0.72	1.04	0.96	0.02
	extreme	4.77	5.26	4.01	4.78	3.87	4.65	0.92	1.33	0.96	0.05
Mid tide +1m	moderate	0.96	1.16	1.00	1.14	0.83	0.93	0.50	0.66	0.83	0.16
	high	2.25	2.54	2.45	2.78	2.29	2.61	0.73	1.06	0.94	0.08
	storm	3.85	4.49	3.77	4.45	3.54	4.14	1.06	1.66	0.94	0.06
	extreme	5.55	6.37	4.87	5.84	4.65	5.57	1.28	1.73	0.96	0.06
High tide	moderate	1.20	1.44	1.31	1.54	0.91	1.10	0.82	1.00	0.70	0.22
	high	2.27	2.52	2.57	2.98	2.23	2.49	1.14	1.64	0.87	0.12
	storm	3.95	5.37	4.11	4.58	3.67	4.04	1.64	2.29	0.89	0.10
	extreme	5.55	6.70	5.32	6.36	4.85	5.91	1.82	2.79	0.91	0.13

Considering $R_{2\%}$ exceedance at high tide, we observe that $R_{2\%}$ can be highly variable in the longshore direction. In order to show the absolute $R_{2\%}$ longshore variability, runup is denoted $\overline{R}_{2\%}$-$R_{2\%min}$ | $\overline{R}_{2\%}$ | $R_{2\%max}$-$\overline{R}_{2\%}$. For low condition $R_{2\%}$ = 0.24 m | 1.20 m | 0.23 m; for moderate conditions $R_{2\%}$ = 0.30 m | 2.27 m | 0.25 m; for storm conditions $R_{2\%}$ = 0.45 m | 3.95 m | 1.41 m and for extreme conditions $R_{2\%}$ = 0.60 m | 5.55 m | 1.15 m. From simulations alongshore variability of $R_{2\%}$ is so observed between 24 and 47 % on average 35% of $\overline{R}_{2\%}$. Runup in the hot spot, can be 11 to 36% higher than $\overline{R}_{2\%}$ are in average 22% higher.

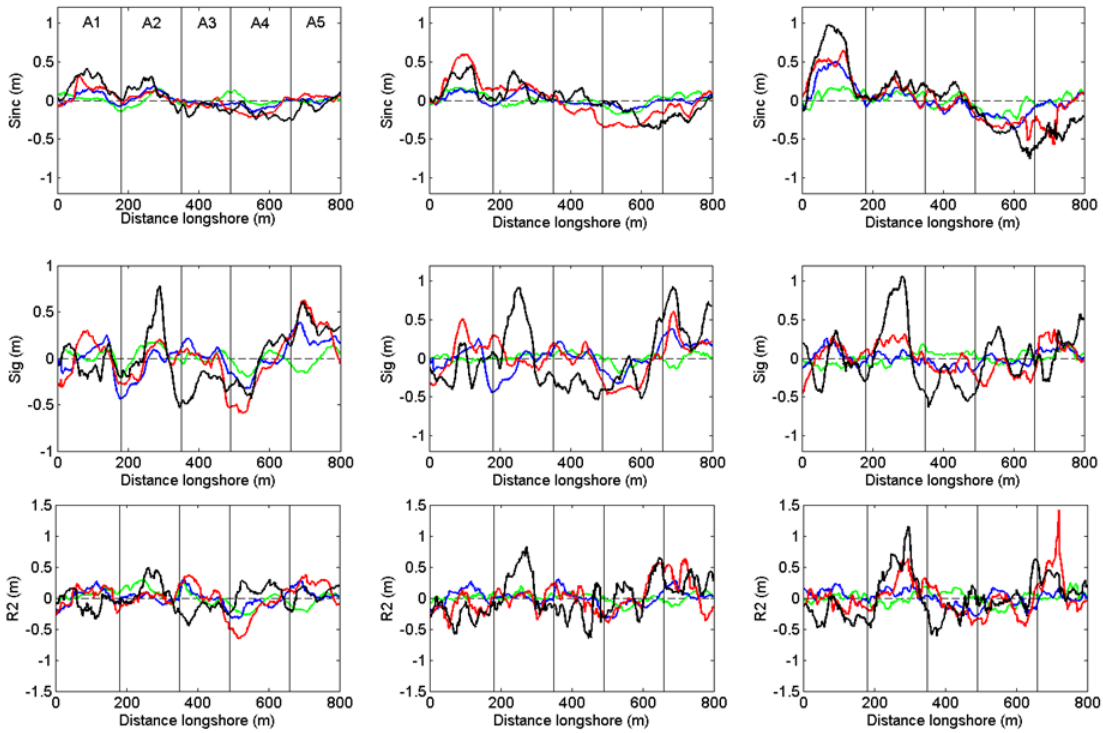

Figure 4 : Longshore local anomaly of S_{inc}, S_{ig}, $R_{2\%}$ relative to respective longshore mean value. Left panel for mid-tide, center for mid-tide + 1m, right panel for high tide. Curve color: green for moderate conditions, blue for high conditions, red for storm conditions and black for extreme conditions.

The question of spatial variability of wave setup and wave runup was addressed by Stockdon et al. (2006), observing results of Duck 94 field experiment for waves reaching 4 m. Observations showed that spatial variations are related to the 3D morphology and increase as the morphology became more marked. In this case *S* showed longshore variability around 0.4 m to 0.5 m which is comparable with our simulated results for moderate conditions $S = 0.25\ \text{m} \mid 1.31\ \text{m} \mid 0.25\ \text{m}$, and partly for high conditions $S = 0.25\ \text{m} \mid 2.57\ \text{m} \mid 0.41\ \text{m}$ (cf. figure 4). For more energetic conditions the *S* longshore variability continues to increase reaching around 1 m for storm conditions and more than 1.5 m under extreme conditions. Even if wave conditions are notably different, these results concur more with Ruggiero et al. (2004) and Guedes et al. (2011) who observed longshore runup variability on field. They assessed alongshore changes in runup of up to a factor of 2 during highly dissipative conditions on a multiple-barred, low-sloping beach and for moderate wave conditions on a steep barred beach.

3.3. *Swash energy spectra*

Longshore mean swash energy spectra are illustrated (fig. 5). They present significant contrasted behavior function of the off-shore wave energy conditions and the tidal water level. Generally, the simulated short wave energy spectra for Hz > 0.05, exhibit a f^{-3} - f^{-4} energy roll-off behavior in agreement with theoretical findings (Huntley et al., 1977; Baldock and Holmes, 1999) and field observations (Guza and Feddersen, 2012; Ruessink et al., 1998; Ruggiero et al., 2004). In some cases, we observe that energy roll-off can vary between f^{-4} and f^{-3}. The energy roll-off appears more f^{-4} dependent at mid-tide and more f^{-3} dependent at high tide (e.g. fig 5c). For moderate wave conditions, main spectral characteristics evolve from generally dissipative spectra at mid-tide to a reflective spectra shape at high tide. It is surprising that at high tide for moderate conditions, longshore mean spectra present characteristics of a reflective beach state (well defined short wave swash energy peak and a peak at first sub-harmonic energy level). For this case, the longshore mean ratio S_{ig}/S_{inc} is about 70 % and do not pass under 60 % indicating more appropriately an intermediate/dissipative beach state. Nevertheless as explain in section 3.1 this reflective shape is mostly due to steep local beach slope at high tide. Another remarkable point is that at mid-tide, considering the conventional frequency cut-off , the roll-off band extends deeply into infragravity frequencies (0.037 Hz) illustrating the highly dissipative conditions at mid-tide due to interactions with the well-developed inner bar system, see (fig 1). Moreover a peaky structure probably caused by accentuated surf zone morphology and resonance effect is observable.

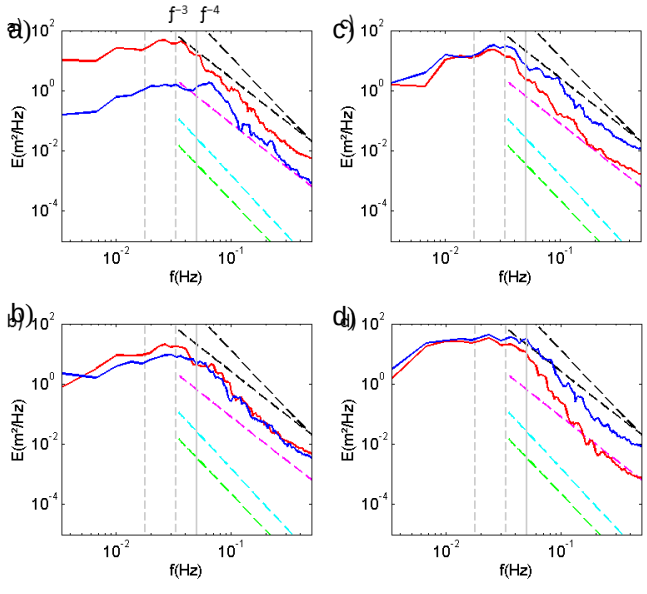

Figure 5 : Swash energy spectra for moderate (a), medium (b), high (c) and extreme (d) wave energy conditions and for mid tide (red line) and high tide water level (blue line). Black dashed lines represent a f^{-4} and f^{-3} energy roll-off. Dashed lines represent the best linear fits to estimate energy roll-off from observations of Ruessink et al., 1998 (Magenta) and Ruggiero et al., 2004 (green and cyan). The vertical grey lines from right to left indicate the division between the infragravity and the sea swell frequency bands (at 0.05 Hz), between high infragravity and mid infragavity bands (0 .033 Hz) and between mid and lowest infragravity band (0 .018 Hz) from Ruessink et al. (1998).

For highly energetic waves, tidal control appears to be less important and conditions are generally dissipative considering S_{ig}/S_{inc}. Nevertheless we note that at high tide the shape of the spectra exhibits more clearly intermediate beach-state shape in reference to Hugues classification with a roll-off limited to 0.05Hz. For storm conditions, the general shape is dissipative with a particularly deep roll-off band which extends into infragravity frequencies (0.027 and 0.033 Hz) and the resonant peaky structures are still observable. The main difference between mid-tide and high tide is the increase in incident energy level (short wave energy level), mainly due to the increase in the local beach slope values at high tide. S_{inc} increases of more than a factor of 2 whereas S_{ig} only increases by 10%. For extremes wave conditions, we observe all the characteristics of a highly dissipative beach state. Similarly to classic storm conditions, the clearest differences between mid-tide and high tide are the increase in incident energy level. The infragravity part of the spectra is quite featureless tending to a nearly parabolic shape, indicating that peaks potentially related to resonant frequencies tend to be less significant.

4. Discussion

Considering that overall, the most accurate parametric models based on extensive field data sets reproduce observed $R_{2\%}$ with error of about 25%. (Atkinson et al., 2017), performance provided by our hybrid models (based on observations on open barred beach from the bibliography and simulated results) are quite satisfactory to estimate runup from extreme wave conditions for such a beach system (mean error about 35% for S_{ig} and about 31% for $R_{2\%}$).

One of the limitation of a parametric model is that it cannot account for the alongshore runrup variability that may occur for identical offshore wave conditions. As we observed, part of the runup is highly correlated to the local beach slope. Nevertheless the local beach slope alone does not fully explain the runup. Qualitatively, we observe that subtidal morphology can influence in part energy dissipation mostly under storm and extreme wave conditions. Infragravity swash can be responsible of hot spot of runup related to the morphology of the outer bar. However, as reported by Cohn and Ruggiero (2016), identifying a pertinent morphodynamic descriptor of parameters influencing swash processes at infragravity frequencies appears to be challenging and an ongoing research matter.

We analyse the progression of the spectra at high tide under increasing wave energy (fig. 6). Generally, the results follow the idealized evolutionary sequence of swash spectra under rising conditions proposed by Hugues et al. (2014). Qualitatively, spectra are evolving from reflective for moderate wave conditions, to intermediate for high conditions and dissipative for storm and extreme wave conditions. The incident band spectra follow a f^{-4} energy roll-off and the increase in energy level is mainly due to the increase in the local beach slope. For moderate wave conditions a short wave energy peak is well defined and progressively the roll-off extends into the infragravity band if conventional limit between Sinc and Sig is considerate. Nevertheless, it is relevant to note that considering a cut off frequencies based on off-shore wave conditions like 2**Tp* (more adapted for very long offshore wave conditions) suggest that no significant saturation is observable at infragravity frequencies.

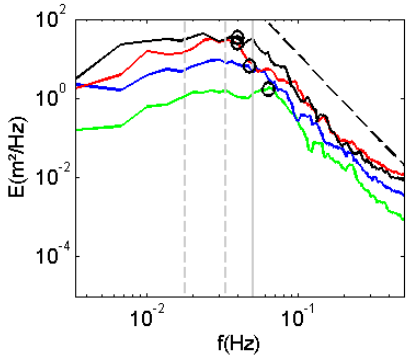

Figure 6 : Swash energy spectra for moderate (green line), high (blue line), stormy (red line) and extreme (black line) wave energy conditions at high tide water level. Black dashed lines represent a f^{-4} energy roll-off and the circles denote the lowest saturated frequency. The vertical lines from right to left indicate the division between the infragravity and the sea swell frequency bands (at 0.05 Hz), between high infragravity and mid infragavtity bands (0 .033 Hz) and between mid and lowest infragravity bands (0 .018 Hz) from Ruessink et al. (1998).

We also observe some behavior not specifically documented in Hugues et al. (2014). For example, for extreme wave conditions, frequencies between 0.1 and 0.05 Hz show a notable increase in energy. This behavior must be further investigated but can be related to non-linear energy transfer back from infragravity to incident band due to interaction with the dune front, infragravity wave breaking (Battjes et al., 2004; de Bakker et al., 2014) and to energy transfer from infragravity to incident wave frequencies (Henderson et al., 2006; Thomson et al., 2006) due to self-self-interactions of the infragravity waves in very shallow water. Another particular behavior is the peaky structures observable in infragravity bands (fig. 6) and particularly clear for storm wave conditions (6 m, 16 s). These peaks are considered to be related to resonant effect (Kirby et al., 1981; Wright, 1982). In field, due to intense wave conditions during storms, near shore bar morphology tends to rapidly evolve and to become more subdued. The expected effect is a less significant resonance effect in the surf zone and therefore a smaller peak at infragravity frequencies. Due to the use of a fixed bathymetry for all simulated cases, the peaky structure for most energetic wave conditions is probably accentuated artificially. Nevertheless, observation of the runup energy spectra in (Senechal et al., 2011) during a major storm at Truc Vert Beach showed a significant peak at infragravity frequencies before, at the apex and even after the storm. These observations can support the fact that at the temporal scale of a storm, morphological evolution may not be sufficient to totally prevent preferential amplifications at infragravity frequencies. These peaks can also be related to OBS morphology the evolutions of which are slower.

5. Conclusion

The analysis of the runup behavior, considering the incident and infragravity swash heights and the 2% runup, under increasing wave and water level conditions show that the increase in tide water level is responsible of an accentuated longshore variability (difference between longshore min and max values) whatever the offshore wave conditions. At high tide, alongshore variability of $R_{2\%}$ is observed between 24 and 47 % and on average 35% of $\overline{R}_{2\%}$. Maximum $R_{2\%}$ in the hot spot, can be 11 to 36% higher than $\overline{R}_{2\%}$ and are in average 22% higher.

As reported in many studies, incident swash is strongly correlated with local intertidal slope and infragravity swash with $(HoLo)^{1/2}$. For moderate and for highly energetic wave conditions, simulated results are of the same order of magnitude than observations collected in several barred open ocean beaches. Nevertheless parametric models from the bibliography generally underestimate simulated results from storm and extreme conditions. The proposed models (based on observations on open barred beach from the bibliography and simulated results) present satisfactory results to estimate S_{ig} and $R_{2\%}$ runup from extreme wave conditions for such a beach system.

Qualitatively, swash energy spectra are evolving from reflective for moderate conditions, to intermediate for high conditions and dissipative for storm and extreme wave conditions. Nevertheless, the ratio S_{inc}/S_{ig} related to the Iribarren number indicates infragravity dominated reflective beach conditions at high tide, for storm and extreme wave conditions. These results underline that the use of the Iribarren number related to the local foreshore slope may not be relevant to characterize storm regime in multi-barred beach. The characterization of morphological control on runup during highly energetic conditions must be further investigated in order to better identify the role of non-uniform energy dissipation and resonance effect with the near shore morphology in the longshore runup variability.

Acknowledgements
This work was funded by BRGM.

References

Aagaard, T., 1991. Multiple-Bar Morphodynamics and Its Relation to Low-Frequency Edge Waves. *Journal of Coastal Research* 7, 801–813.

Aagaard, T., 1990. Infragravity waves and nearshore bars in protected, storm-dominated coastal environments. *Marine Geology* 94, 181–203. doi:10.1016/0025-3227(90)90069-V

Atkinson, A.L., Power, H.E., Moura, T., Hammond, T., Callaghan, D.P., Baldock, T.E., 2017. Assessment of runup predictions by empirical models on non-truncated beaches on the south-east Australian coast. *Coastal Engineering*

Baldock, T.E., Holmes, P., 1999. Simulation and prediction of swash oscillations on a steep beach. *Coastal Engineering* 36, 219–242.

Battjes, J.A. 1974, "Surf similarity", *Proceedings 14th International Conference on Coastal Engineering*, pp.466–480

Battjes, J.A., Bakkenes, H.J., Janssen, T.T., van Dongeren, A.R., 2004. Shoaling of subharmonic gravity waves. *J.*

Geophys. Res. 109, C02009.
Brinkkemper, J.A., Torres-Freyermuth, A., Mendoza, E.T., Salles, P., Ruessink, B.G., 2013. Parameterization of wave run-up on beaches in Yucatan, Mexico: a numerical study, *Coastal Dynamic 2013*.
Castelle, B., Bonneton, P., Dupuis, H., Sénéchal, N., 2007. Double bar beach dynamics on the high-energy meso-macrotidal French Aquitanian Coast: A review. *Marine Geology* 245, 141–159.
Castelle, B., Marieu, V., Bujan, S., Splinter, K.D., Robinet, A., Sénéchal, N., Ferreira, S., 2015. Impact of the winter 2013–2014 series of severe Western Europe storms on a double-barred sandy coast: Beach and dune erosion and megacusp embayments. *Geomorphology* 238, 135–148.
Cohn, N., Ruggiero, P., 2016. The influence of seasonal to interannual nearshore profile variability on extreme water levels: Modeling wave runup on dissipative beaches. *Coastal Engineering, Swash-zone Processes* 115, 79–92.
Cox, N., Dunkin, L.M., Irish, J.L., 2013. An empirical model for infragravity swash on barred beaches. *Coastal Engineering* 81, 44–50.
de Bakker, A.T.M., Tissier, M.F.S., Ruessink, B.G., 2014. Shoreline dissipation of infragravity waves. *Continental Shelf Research* 72, 73–82.
Guedes, R.M.C., Bryan, K.R., Coco, G., 2012. Observations of alongshore variability of swash motions on an intermediate beach. *Continental Shelf Research* 48, 61–74.
Guedes, R.M.C., Bryan, K.R., Coco, G., Holman, R.A., 2011. The effects of tides on swash statistics on an intermediate beach. *J. Geophys. Res.* 116, C04008.
Guza, R.T., Feddersen, F., 2012. Effect of wave frequency and directional spread on shoreline runup. *Geophys. Res. Lett*. 39, L11607.
Guza, R.T., Thornton, E.B., 1982. Swash oscillations on a natural beach. *J. Geophys. Res.* 87, 483–491.
Henderson, S.M., Guza, R.T., Elgar, S., Herbers, T.H.C., Bowen, A.J., 2006. Nonlinear generation and loss of infragravity wave energy. *J. Geophys. Res.* 111, C12007.
Holman, R.A., 1986. Extreme value statistics for wave run-up on a natural beach. Coastal Engineering 9, 527–544.
Hughes, M.G., Aagaard, T., Baldock, T.E., Power, H.E., 2014. Spectral signatures for swash on reflective, intermediate and dissipative beaches. *Marine Geology* 355, 88–97.
Huntley, D.A., Guza, R.T., Bowen, A.J., 1977. A universal form for shoreline run-up spectra? *J. Geophys. Res*. 82, 2577–2581.
Kirby, J.T., Dalrymple, R.A., Liu, P.L.-F., 1981. Modification of edge waves by barred-beach topography. *Coastal Engineering* 5, 35–49.
Masselink, G., Short, A.D., 1993. The Effect of Tide Range on Beach Morphodynamics and Morphology: A Conceptual Beach Model. *Journal of Coastal Research* 9, 785–800.
Miche, R., 1951. Le pouvoir réfléchissant des ouvrages maritimes exposes à l'action de la houle. Annales des Ponts et Chausses 121, 285–319.
Nicolae Lerma A., Pedreros R., Robinet A., Sénéchal N., 2017. Simulating wave setup and run-up during storm conditions on a complex barred beach, *Coastal Engineering*, 123 29–41.
Ruessink, B.G., Kleinhans, M.G., van den Beukel, P.G.L., 1998. Observations of swash under highly dissipative conditions. *J. Geophys. Res*. 103, 3111–3118.
Ruggiero, P., Holman, R.A., Beach, R.A., 2004. Wave run-up on a high-energy dissipative beach. *J. Geophys. Res.* 109, C06025.
Sallenger, A.H., Holman, R.A., 1985. Wave energy saturation on a natural beach of variable slope. *J. Geophys. Res*. 90, 11939–11944.
Senechal, N., Coco, G., Bryan, K.R., Holman, R.A., 2011. Wave runup during extreme storm conditions. *J. Geophys. Res.* 116, C07032.
Senechal, N., Coco, G., Plant, N., Bryan, K., 2014. Variabilité longitudinale du jet de rive en présence de conditions dissipatives. Editions Paralia, pp. 177–184. doi:10.5150/jngcgc.2014.020
Sénéchal, N., Gouriou, T., Castelle, B., Parisot, J.-P., Capo, S., Bujan, S., Howa, H., 2009. Morphodynamic response of a meso- to macro-tidal intermediate beach based on a long-term data set. *Geomorphology* 107, 263–274.
Stockdon, H.F., Holman, R.A., Howd, P.A., Sallenger Jr., A.H., 2006. Empirical parameterization of setup, swash, and runup. *Coastal Engineering* 53, 573–588.
Thomson, J., Elgar, S., Raubenheimer, B., Herbers, T.H.C., Guza, R.T., 2006. Tidal modulation of infragravity waves via nonlinear energy losses in the surfzone. *Geophys. Res. Lett.* 33, L05601.
Wright, L.D., 1982. Field observations of long-period, surf-zone standing waves in relation to contrasting beach morphologies. *Mar. Freshwater Res*. 33, 181–201.
Wright, L.D., Short, A.D., 1984. Morphodynamic variability of surf zones and beaches: A synthesis. *Marine Geology* 56, 93–118.
Zijlema, M., Stelling, G.S., Smit, P.B., 2011. SWASH: an operational public domain code for simulating wave fields and rapidly varied flows in coastal waters, *Coastal Engineering* 58 992–1012.